

Short pulse generation from a graphene-coupled passively mode-locked terahertz laser

In the format provided by the authors and unedited

Supplementary Information

Table of Contents:

- I. Flowchart of the fabrication process
- II. Measurement of the refractive index in multilayer graphene (MLG)
- III. DGSA-QCL with different cavity dimensions and MLG thickness
- IV. Micro-Raman characterization

I. Flowchart of the fabrication process

Figure S1 shows the flowchart of the device fabrication process. The active region (AR), grown on a host GaAs wafer, is first wafer-bonded face down, by thermo-compression, to a highly doped GaAs substrate, with a 1 μ m-thick Au middle layer (Figure S1a). This step is essential to define a double metal waveguide. The host AR GaAs substrate is then removed by mechanical lapping and chemical etching (Figure S1b). The AR is hence ready for the optical lithography and thermal evaporation of the Au top contact (patterned to host the DGSA) and Ni side absorbers (Figure S1c). After the metallization, vertical sidewalls are defined by inductively coupled plasma (ICP) etching (Figure S1d): this process allows us to obtain vertical sidewalls. The double metal QCL is ready for MLG wet transfer (Figure S1e). MLG is then lithographically patterned and oxygen plasma etched, to cover only the DGSA (Figure S4f). At the end of the fabrication process, the GaAs substrate is lapped down to 150 nm and covered by Au (Figure S1g), to improve thermal management and enable CW operation.

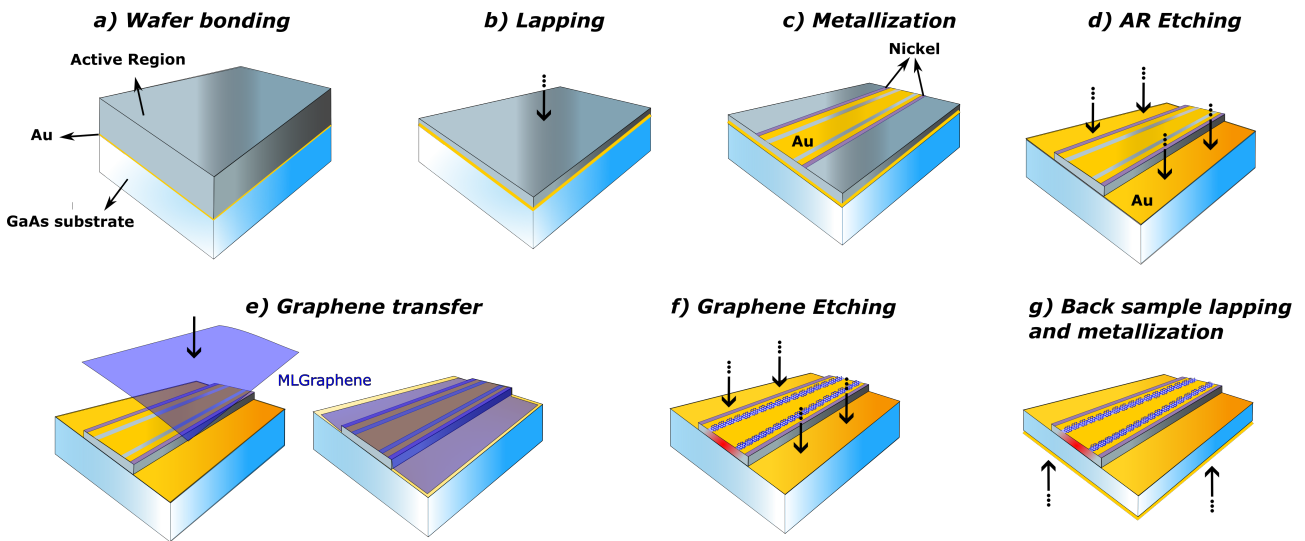


Figure S1: Schematic of the DGSA-QCL fabrication process

II. Measurement of the refractive index in multilayer graphene (MLG)

The electromagnetic simulations of the DGSA include the frequency dependent complex refractive index of MLG, implemented into Comsol Multiphysics as a transition boundary condition at the interface between highly doped GaAs layer and air, into the stripes etched in the top Au contact. A part of the MLG transferred onto the waveguide stripes is also transferred onto an undoped GaAs substrate to be characterized with a THz-TDS setup (Tera K5 by Menlo-Systems). About one half

of the substrate was left uncoated to be used as reference. The graphene conductivity $\tilde{\sigma}_g(\omega)$ was measured in the 0.4–2.2 THz range as for Ref. ¹, giving DC conductivity $\sigma_{DC} = 1.72$ mS and scattering time $\tau = 68$ fs for the corresponding Drude fit.

The DC conductivity can be written as $\sigma_{DC} = \frac{2e^2}{h} |k_F| v_F \tau$, where $k_F = \sqrt{\pi n}$, $v_F \sim 1.2 \times 10^6$ m/s is Fermi velocity. These values lead to $E_{F=} = 0.2 \pm 0.03$ eV, in accordance with the Raman spectroscopy results. We compute the MLG permittivity $\tilde{\epsilon}_g(\omega)$ from:

$$\tilde{\epsilon}_g(\omega) = 1 - \frac{i\tilde{\sigma}_g(\omega)}{(\omega\epsilon_0 d_g)}$$

with d_g the MLG thickness (7×0.335 nm = 2.345 nm)² and ϵ_0 the vacuum dielectric constant. The MLG refractive index $\tilde{n}_g(\omega) = \sqrt{\tilde{\epsilon}_g(\omega)}$ can then be extracted from the dielectric constant and its value extrapolated in the QCL emission band, Fig. S2.

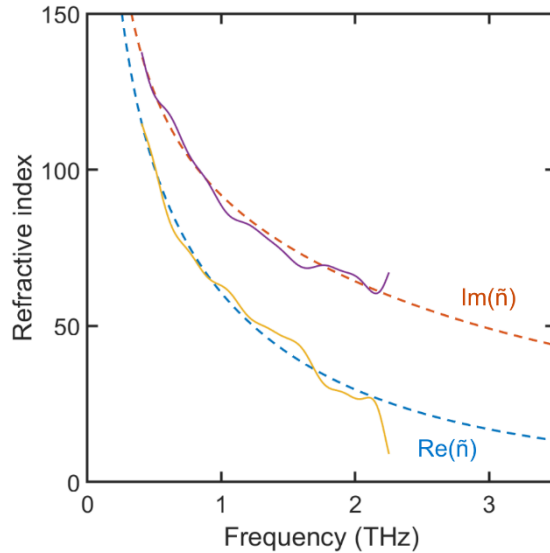


Figure S2: complex refractive index of 7LG on GaAs.

Real and imaginary parts of experimental refractive index of MLG on undoped GaAs (purple and orange curves) from 0.4 to 2.2 THz. The red and blue curves are the Drude model fit with $\sigma_{DC} = 1.72$ mS and $\tau = 68$ fs, extrapolated into the QCL emission band, yielding a complex refractive index $\tilde{n}_g(3 \text{ THz}) = 16.9 + i 49.2$.

III. DGSA-QCL with different cavity dimensions and MLG thickness

The beatnote linewidth reduction observed in Fig. 2d is consistently observed in QCLs with the DGSA and never seen in reference QCLs fabricated with the same active region^{3–5}. Fig. S3a shows a THz QCL fabricated with the same active region of the device in the main text, but having different cavity dimensions ($3.13\text{mm} \times 68\mu\text{m} \times 17\mu\text{m}$), the stripes at ~ 20 μm from the cavity longitudinal axis and a 15LG SA. Its L-I-V characteristic (Fig. S3b) has the same threshold current density and a slightly larger CW optical power (~ 10.5 mW) compared to the device presented in the

main text, due to its wider cavity. The intermodal beatnote map (Fig. S3d) reveals that, as for the QCLs with DGSA in the main text, there are two regions in which the beatnote is single and narrow ($\sim 10^3$ Hz) (Fig. S2e); one extending for 100 mA just above threshold (left shaded light blue area in Fig. S3b) and the other before and across the NDR (right shaded light blue area in Fig. S3b).

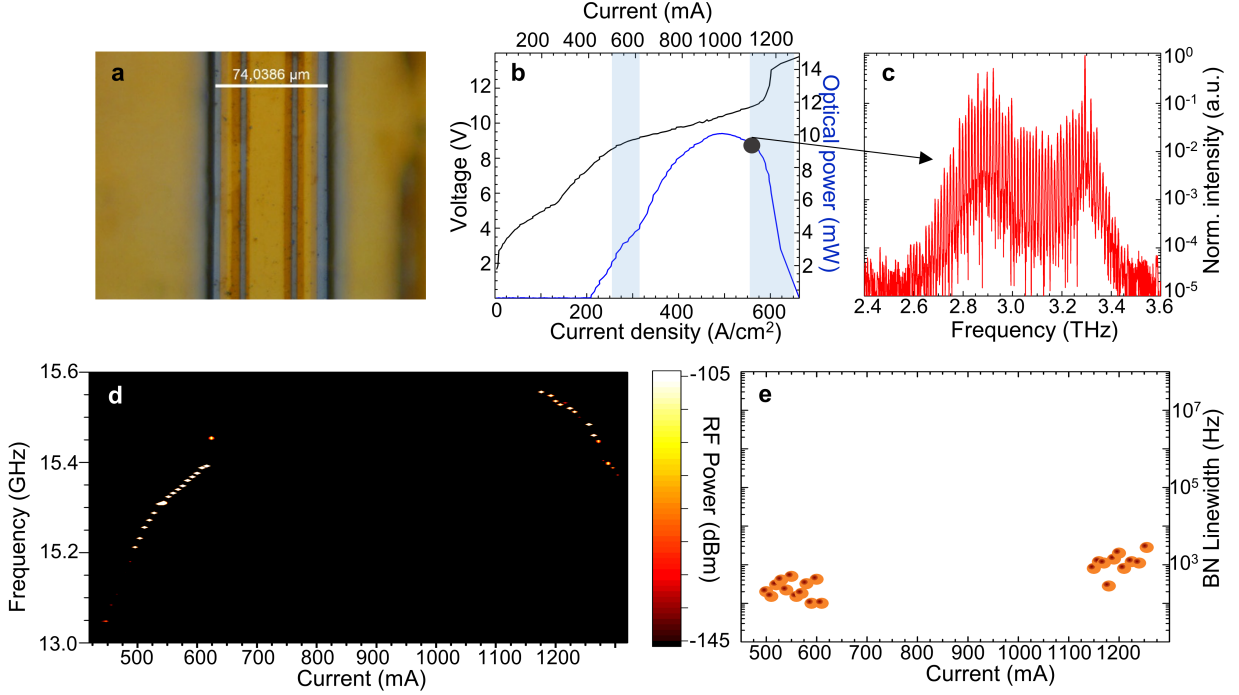


Figure S3: Electro-optical characterization of 15LG DGSA-QCL.

a. DGSA-QCL with a cavity of $3.13\text{mm} \times 68\mu\text{m} \times 17\mu\text{m}$ and 15LG-covered stripes at $20\mu\text{m}$ from the QCL longitudinal axis. **b.** CW light current voltage characteristics of the same device. The blue shaded areas are the bias ranges where the beatnote linewidth is $\sim 10^3$ Hz. The black dot is the bias point corresponding to the spectrum in Fig. S2C. **c.** FTIR spectrum acquired by biasing the DGSA-QCL at 1100 mA with a heat-sink temperature of 20 K. **d.** Beatnote map of the DGSA-QCL in its operating range. **e.** Intermodal beatnote linewidth plotted as a function of driving current.

IV. Micro-Raman characterization

Micro Raman measurements are performed on the CVD SLG and on the MLG sample transferred on the QCL top contact (Fig. S4a). We use a confocal Raman spectrometer (Horiba, Explora Plus) equipped with a $100\times$ objective at 532 nm, producing a laser spot size of $\sim 0.5\mu\text{m}$. The Raman spectrum of the SLG, plotted in Fig. S4b (black), shows two intense peaks, typically retrieved in graphene⁶, i.e the G (1583cm^{-1} , $\text{FWHM} = 13\text{cm}^{-1}$) and the 2D (2690cm^{-1} , $\text{FWHM} = 25\text{cm}^{-1}$) peak. As expected in SLG, the 2D peak can be fitted by a single Lorentzian. The intensity and area ratios of 2D and G peak are $I(2D)/I(G) \sim 2.9$ and $A(2D)/A(G) \sim 4.8$, respectively. This corresponds to $E_F \sim 0.23\text{eV}$ and p -type doping^{7,8}.

To additional Raman peaks can be retrieved in the spectrum of the MLG sample (Fig. S4, blue), e.g. the D (1344 cm^{-1} , $\text{FWHM} = 67\text{ cm}^{-1}$) and D' (1616 cm^{-1} , $\text{FWHM} = 24\text{ cm}^{-1}$) peaks. They arise from defect-assisted Raman processes^{6,9}, reflecting the disorder introduced during the multiple graphene transfer steps. Despite this, the D- and G- peak intensities ratio indicates a negligible defect density.

The 2D band in the MLG sample is always single-peaked, but broader ($\text{FWHM} = 34\text{ cm}^{-1}$). The intensity and area ratios of 2D and G peak are reduced with respect to the SLG ($I(2D)/I(G) \sim 1.6$ and $A(2D)/A(G) \sim 2.8$). This is indicative of a rotationally disordered MLG¹⁰. The G peak frequency, taken at several different points on the MLG, is close to the value of the SLG, indicating that no significant doping is introduced during the transfer process.

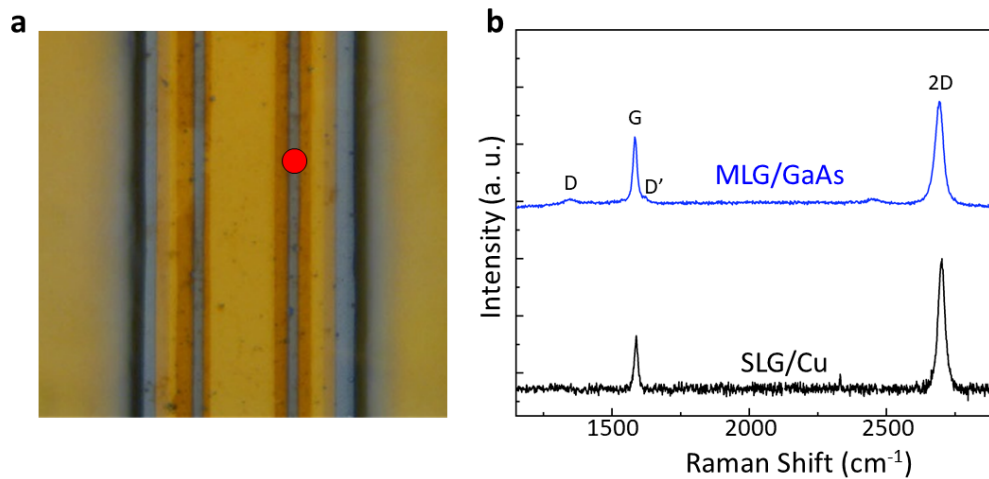


Figure S4: Raman spectra of the graphene samples.

a, Optical microscopy image of the QCL top contact with the MLG stripes. The red dot marks one of the points in which the Raman spectrum have been acquired. **b**, Raman spectra at 532 nm of the as-grown SLG on Cu (black) and of the transferred MLG onto the Ga stripes (blue).

References

1. Buron, J. D. *et al.* Graphene Conductance Uniformity Mapping. *Nano Lett.* **12**, 5074–5081 (2012).
2. Cooper, D. R. *et al.* Experimental Review of Graphene. *ISRN Condens. Matter Phys.* **2012**, e501686 (2012).

3. Garrasi, K. *et al.* High Dynamic Range, Heterogeneous, Terahertz Quantum Cascade Lasers Featuring Thermally Tunable Frequency Comb Operation over a Broad Current Range. *ACS Photonics* **6**, 73–78 (2019).
4. Mezzapesa, F. P. *et al.* Terahertz Frequency Combs Exploiting an On-Chip, Solution-Processed, Graphene-Quantum Cascade Laser Coupled-Cavity. *ACS Photonics* **7**, 3489–3498 (2020).
5. Gaspare, A. D. *et al.* Tunable, Grating-Gated, Graphene-On-Polyimide Terahertz Modulators. *Adv. Funct. Mater.* **31**, 2008039 (2021).
6. Ferrari, A. C. *et al.* Raman Spectrum of Graphene and Graphene Layers. *Phys. Rev. Lett.* **97**, 187401 (2006).
7. Basko, D. M., Piscanec, S. & Ferrari, A. C. Electron-electron interactions and doping dependence of the two-phonon Raman intensity in graphene. *Phys. Rev. B* **80**, 165413 (2009).
8. Das, A. *et al.* Monitoring dopants by Raman scattering in an electrochemically top-gated graphene transistor. *Nat. Nanotechnol.* **3**, 210–215 (2008).
9. Eckmann, A. *et al.* Probing the Nature of Defects in Graphene by Raman Spectroscopy. *Nano Lett.* **12**, 3925–3930 (2012).
10. Lenski, D. R. & Fuhrer, M. S. Raman and optical characterization of multilayer turbostratic graphene grown via chemical vapor deposition. *J. Appl. Phys.* **110**, 013720 (2011).